Conservative Full-Potential Model for Unsteady Transonic Rotor Flows

Roger C. Strawn* and Francis X. Caradonna*
U. S. Army Aeroflightdynamics Directorate, NASA Ames Research Center, Moffett Field, California

A computer program has been developed to solve a three-dimensional conservative formulation of the full-potential equation. Its ability to solve transonic, unsteady rotor flows is demonstrated by comparison to forward flight nonlifting pressure data at low to moderate advance ratios. A "split potential" formulation has been added to the code that incorporates known vorticity fields into the full-potential calculation. Using this methodology, rotor-wake contributions have been incorporated into the computer code. Pressure results are presented for lifting rotors in hover. These results are compared to experimental data as well as to other predictions.

Nomenclature

$\mathcal{R}$ = aspect ratio, R/c
c = rotor chord length
C_p = pressure coefficient
G = prescribed velocity potential
h = nondimensional time step
I = identity matrix
J = Jacobian of coordinate transform matrix
M_T = tip Mach number
n = superscript representing current time level
r = radial distance along the rotor
R = radial distance to the rotor tip
t = nondimensional time
U = contravariant velocity normal to the η,ζ plane
V = contravariant velocity normal to the ξ,ζ plane
W = contravariant velocity normal to the ξ,η plane
X = chordwise distance along the rotor
$\hat{\beta}$ = $\rho^{2-\gamma}/J$
Γ = jump in potential across the wake
γ = specific heat ratio
μ = rotor advance ratio
Φ = total velocity potential
ϕ = perturbation velocity potential
ψ = rotor azimuthal angle, deg
ρ = fluid density normalized by freestream values
$\hat{\rho}$ = ρ/J
θ_c = rotor collective angle, deg

Introduction

MANY modern high performance helicopters are limited by the occurrence of transonic flow on the advancing rotor. The ability to predict this flow is central to the control of high-speed losses, vibration, and noise.

At present, a wide variety of schemes to predict such flows are being developed. These range from panel methods to Euler equation methods. Unsteady potential methods are a reasonable compromise between the two extremes because the shock strength in rotor flows is typically insufficient to generate sizeable vorticity.

Presented as Paper 86-0079 at the AIAA 24th Aerospace Sciences Meeting, Jan. 6-9, 1986; received Feb. 5, 1986; revision received July 1, 1986.

*Research Scientist, AVSCOM. Member AIAA.

There are a wide variety of approaches being employed among the potential methods. Caradonna and Phillippe[1] and Phillippe and Chattot[2] have used an unsteady conservative small-disturbance approach. While quite useful, these methods are limited to low lift and do not accurately handle the lower transonic region. A number of nonconservative full-potential schemes have also been developed (e.g., Arieli and Tauber[3] and Chang and Tung[4]). These methods, however, have trouble predicting the shock motion accurately, particularly in regions with decelerating flow.

The first intent of this paper is to present a three-dimensional, unsteady, conservative, full-potential rotor (FPR) treatment. The FPR code is based on the fixed-wing code of Bridgeman et al.[5] Sankar and Prichard[6] have concurrently developed their own version of a conservative full-potential rotor code. Their formulation is similar, although significant differences exist in the grid type, metric differencing, and formulation of the boundary conditions.

The second objective of this paper is to incorporate a wake-modeling scheme into our full-potential code. A wake-modeling scheme is important since a realistic rotor blade operates in a flowfield whose complexity does not occur in the fixed-wing case. Vortices from preceding blades interact with advancing blades, and these interactions have a large effect on aerodynamic blade loading. Blade-vortex interaction results with the FPR code for hovering rotor cases will be shown. Results for unsteady advancing blades are given in Ref. 7. Egolf and Sparks[8] have developed their own method for incorporating rotor wakes into finite-difference computations for rotors in hover. Direct comparisons will be made between their method and ours.

Formulation of the Full-Potential Equation

The formulation for the FPR code is based on the fixed-wing code of Bridgeman et al.[5] which solves the three-dimensional, full-potential equation in strong conservation form

$$\frac{\partial \rho}{\partial t}+\frac{\partial}{\partial x}(\rho\Phi_x)+\frac{\partial}{\partial y}(\rho\Phi_y)+\frac{\partial}{\partial z}(\rho\Phi_z)=0 \tag{1}$$

with density determined from the Bernoulli equation,

$$\rho=\left[1+\frac{\gamma-1}{2}(-2\Phi_t-\Phi_x^2-\Phi_y^2-\Phi_z^2)\right]^{1/(\gamma-1)} \tag{2}$$

A generalized transformation of the equations is given as follows:

$$\xi=\xi(x,y,z,t) \quad \eta=\eta(x,y,z,t) \quad \zeta=\zeta(x,y,z,t) \quad \tau=t \tag{3}$$

The strong conservation law form of Eq. (1) is maintained in the resulting transformed equation

$$\frac{\partial}{\partial\tau}\left(\frac{\rho}{J}\right)+\frac{\partial}{\partial\xi}\left(\frac{\rho U}{J}\right)+\frac{\partial}{\partial\eta}\left(\frac{\rho V}{J}\right)+\frac{\partial}{\partial\zeta}\left(\frac{\rho W}{J}\right)=0 \tag{4}$$

with density given by

$$\rho=\left\{1+\frac{\gamma-1}{2}\left[-2\Phi_\tau-(U+\xi_t)\Phi_\xi-(V+\eta_t)\Phi_\eta-(W+\zeta_t)\Phi_\zeta\right]\right\}^{1/(\gamma-1)} \tag{5}$$

where

$$U=\xi_t+A_1\Phi_\xi+A_4\Phi_\eta+A_5\Phi_\zeta, \quad V=\eta_t+A_4\Phi_\xi+A_2\Phi_\eta+A_6\Phi_\zeta$$
$$W=\zeta_t+A_5\Phi_\xi+A_6\Phi_\eta+A_3\Phi_\zeta \tag{6}$$

$$A_1=\xi_x^2+\xi_y^2+\xi_z^2, \quad A_2=\eta_x^2+\eta_y^2+\eta_z^2, \quad A_3=\zeta_x^2+\zeta_y^2+\zeta_z^2$$
$$A_4=\xi_x\eta_x+\xi_y\eta_y+\xi_z\eta_z, \quad A_5=\xi_x\zeta_x+\xi_y\zeta_y+\xi_z\zeta_z$$
$$A_6=\eta_x\zeta_x+\eta_y\zeta_y+\eta_z\zeta_z \tag{7}$$

All velocities are normalized by a_∞, distances by the airfoil chord length, and time by the combination (c/a_∞). Density is normalized by the freestream value.

Equation (4) is solved by using first-order backward-differencing in time and second-order central-differencing in space. The temporal density derivative is locally linearized about the old time levels in a manner that preserves the conservative form (see Ref. 5).

The resulting equation is approximately factored into ξ, η, and ζ operators:

$$\left[I+hU^n\delta_\xi-\frac{h^2}{\hat\beta^n}\delta_\xi(\hat\rho A_1)^n\delta_\xi\right]\times\left[I+hV^n\delta_\eta-\frac{h^2}{\hat\beta^n}\delta_\eta(\hat\rho A_2)^n\delta_\eta\right]\times\left[I+hW^n\delta_\zeta-\frac{h^2}{\hat\beta^n}\delta_\zeta(\hat\rho A_3)^n\delta_\zeta\right](\Phi^{n+1}-\Phi^n)$$
$$=\frac{h^2}{\hat\beta^n}[\delta_\xi(\hat\rho U)^n+\delta_\eta(\hat\rho V)^n+\delta_\zeta(\hat\rho W)^n-R_\infty]+C \tag{8}$$

where δ_ξ, δ_η, and δ_ζ represent central-difference operators in space, and the term C is given by Eq. (9). The bracketed term in Eq. (9) represents the temporal conservation correction to the algorithm.

$$C=(\Phi^n-\Phi^{n-1})+\left[\frac{\hat\beta^{n-1}}{\hat\beta^n}(\Phi^n-2\Phi^{n-1}+\Phi^{n-2})+\frac{h}{\hat\beta^n}(\hat\rho^n-\hat\rho^{n-1})+h\frac{\hat\beta^{n-1}}{\hat\beta^n}(U^{n-1}\delta_\xi+V^{n-1}\delta_\eta+W^{n-1}\delta_\zeta)(\Phi^n-\Phi^{n-1})\right] \tag{9}$$

A steady-state alternating direction implicit (ADI) relaxation algorithm can be obtained from Eq. (8) by omitting the unsteady C term on the right-hand side of the equation.

The streamwise flux terms use upwind density biasing in regions of supercritical flow to ensure stability of the algorithm. Details are given in Ref. 5. The quantity R_∞ represents a numerical truncation error term caused by incomplete metric cancellation. Formulation of this correction term is discussed in Ref. 5.

Boundary Conditions for Rotor Flowfields

Rotor flowfields are computed by modifying the time metric terms ξ_t, η_t, and ζ_t in Eqs. (4) and (5). The finite-difference grid is attached to the rotor blade which moves through still air as shown in Fig. 1. Each grid point has an appropriate rotational coordinate velocity field given by ξ_t, η_t, and ζ_t. This results in freestream conditions that are given by $\Phi=0$. An O-grid has been chosen for the basic finite-difference mesh because of its efficient use of grid points.

A flow tangency condition is implemented on the surface of the rotor by setting the normal contravariant velocity W equal to 0. Along the inner boundary plane normal to the rotor, the contravariant velocity V is set equal to η_t.

For lifting cases, the shed vorticity is specified as a jump in potential Γ imposed across the coordinate plane $\xi=0$. This coordinate plane is approximately aligned with the shear layer from the trailing edge. An unsteady transport equation for this potential jump is imposed across the wake. It is derived by assuming that density is continuous across the cut, and can be written as

$$\Gamma_\tau+\langle V\rangle\Gamma_\eta+\langle W\rangle\Gamma_\zeta=0 \tag{10}$$

where $\langle V\rangle$ and $\langle W\rangle$ are the averages of the contravariant velocities above and below the wake.

At the outer grid boundary, a nonreflection boundary condition has been implemented similar to that used in Ref. 9. If we make the assumption that disturbances propagate only in the radial and spanwise directions at the outer boundary of the O-grid, then a local nonreflection boundary condition can be written as

$$\phi_t+(-M_{\hat r}-1)\phi_{\hat r}+M_y\phi_y=0 \tag{11}$$

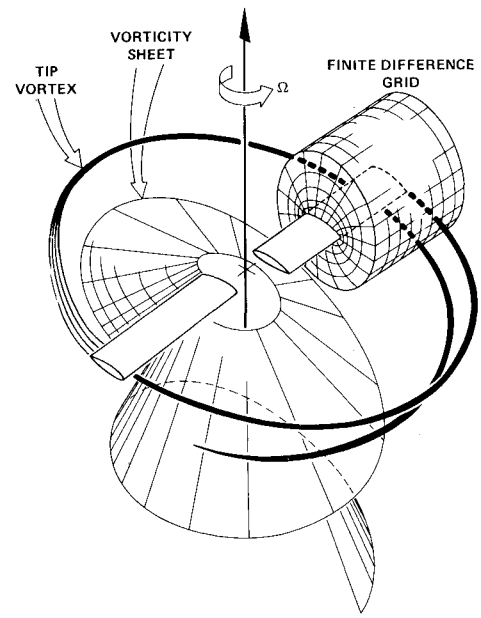

Fig. 1 A rotor-wake system with an embedded finite-difference grid.

where the radial coordinate $\hat{r}$ is normal to the outer surface of the cylindrical O-grid, y is in the rotor spanwise direction along the outer surface of the O-grid, and $M_{\hat{r}}$ and M_y are the freestream Mach number components in the $\hat{r}$ and y directions relative to the blade-fixed grid. A more detailed discussion of the nonreflection boundary condition is given in Ref. 7.

Equation (11) is used explicitly to update the solution on the outer boundary. It is applied after each time-step for the interior points. Implementation of Eq. (11) is necessary for unsteady lifting rotor cases, in order to prevent the accumulation of disturbances at the outer boundary.

Unsteady Rotor Computations

The FPR code described previously was used to compute the nonlifting, unsteady experimental case described by Caradonna et al.[10] This experiment tested a stiff, two-bladed, untwisted, untapered blade with a constant NACA-0012 profile. The blade was pressure-instrumented at $r/R = 0.893$. The two cases considered here are highly supercritical at this pressure station. No wake modeling is required for these cases.

Figure 2 compares computed and experimental results for a blade-tip Mach number of 0.7 and an advance ratio of 0.3. Here, pressure coefficients are plotted at a single radial location for a variety of rotor azimuthal angles. Also shown in these figures are results computed by Tung and Chang[11] with a nonconservative formulation of the potential equation. In both codes, the starting solution was obtained from a quasisteady case that was run at $\psi = 0$ deg.

The two codes agree closely with each other and with the experimental data from $\psi = 0$–120 deg. However, there is a disagreement in the rate of collapse of the shock in the second quadrant. At $\psi = 150$ deg, the Tung and Chang prediction[11] shows a small shock on the rotor. Both the data and the FPR code results indicate that the shock has fully collapsed at this point.

Figure 3 shows computed and experimental results for a blade-tip Mach number of 0.8 and an advance ratio of 0.2. As in the previous case, pressure coefficients are plotted for a series of rotor angles. This case generates a stronger shock on the rotor surface than in the previous case. Agreement of the full-potential results with the data is good from $\psi = 0$–120 deg. At $\psi = 150$ deg, the computer prediction shows the rotor shock collapsing faster than for the data.

These calculations were run with a spanwise series of parallel O-shaped meshes as shown in Fig. 1. There were 81 chordwise points, 19 spanwise points, and 25 grid points normal to the rotor surface. The outer radius for each cylindrical O-grid was located 7 chords from the rotor surface. As close as 4 chords from the rotor surface, computational results show little sensitivity to outer boundary locations.

Typical spanwise grid distributions have inner boundaries located 4 chords from the rotor tip. The initial inboard spacing of the parallel O-grids is 0.5 chords, decreasing to 0.05 chords at the rotor tip. The outer spanwise grid boundary was located approximately 2 chords beyond the tip of the rotor blade. Computational results showed little sensitivity to this boundary location. For the low-aspect-ratio blades computed in this paper, the location of the outer spanwise grid boundary is limited by stability problems that result from freestream supersonic grid velocities. The present density biasing scheme is unable to stabilize the calculation in regions where supersonic flow off the rotor tip is caused only by the motion of grid.

Run times on the NASA Ames Cray XMP 1-2 computer for a 180 deg rotor sweep were approximately 9 CPU minutes. The time-step was fixed at 0.25 deg of rotor motion. At the blade tip, this corresponds to a maximum of ap-

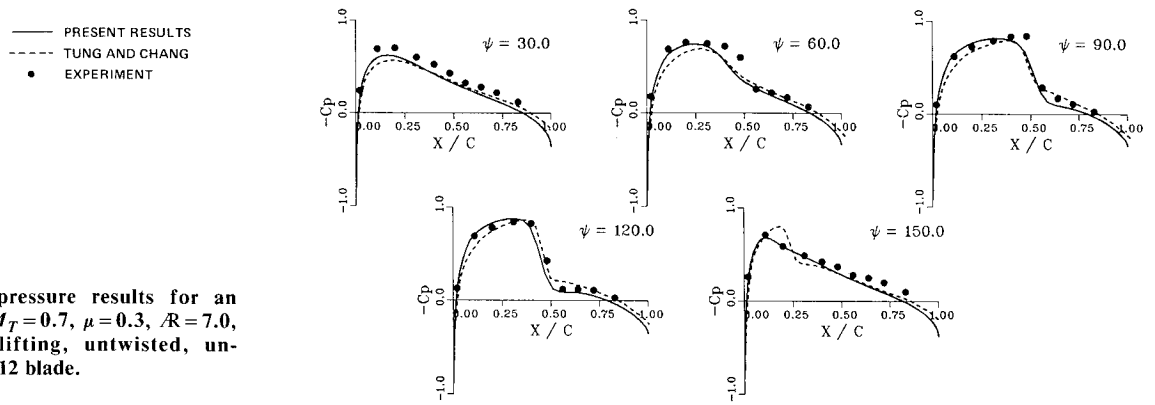

Fig. 2 Surface pressure results for an advancing rotor, $M_T = 0.7$, $\mu = 0.3$, $\mathcal{R} = 7.0$, $r/R = 0.893$, nonlifting, untwisted, untapered, NACA-0012 blade.

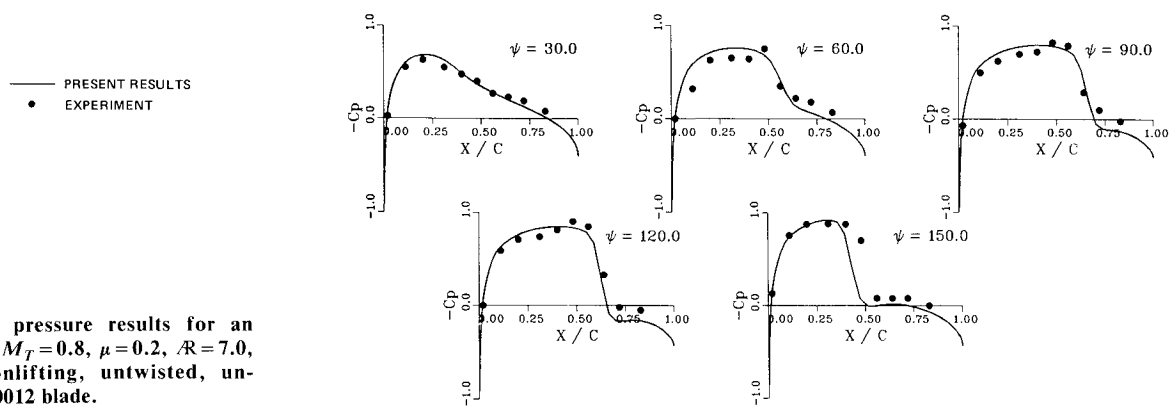

Fig. 3 Surface pressure results for an advancing rotor, $M_T = 0.8$, $\mu = 0.2$, $\mathcal{R} = 7.0$, $r/R = 0.893$, nonlifting, untwisted, untapered, NACA-0012 blade.

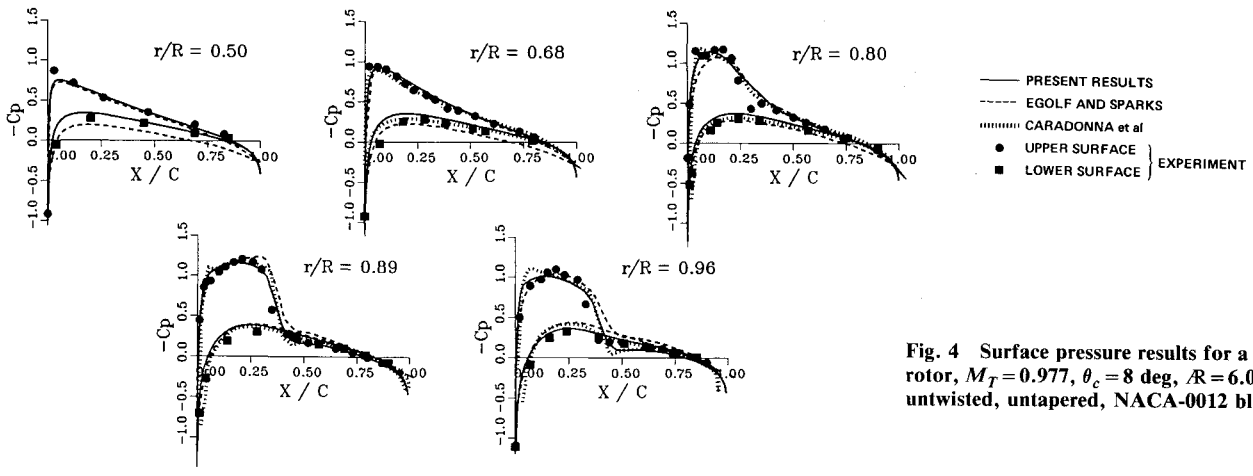

Fig. 4 Surface pressure results for a hovering rotor, $M_T = 0.977$, $\theta_c = 8$ deg, $\mathcal{R} = 6.0$, untwisted, untapered, NACA-0012 blade.

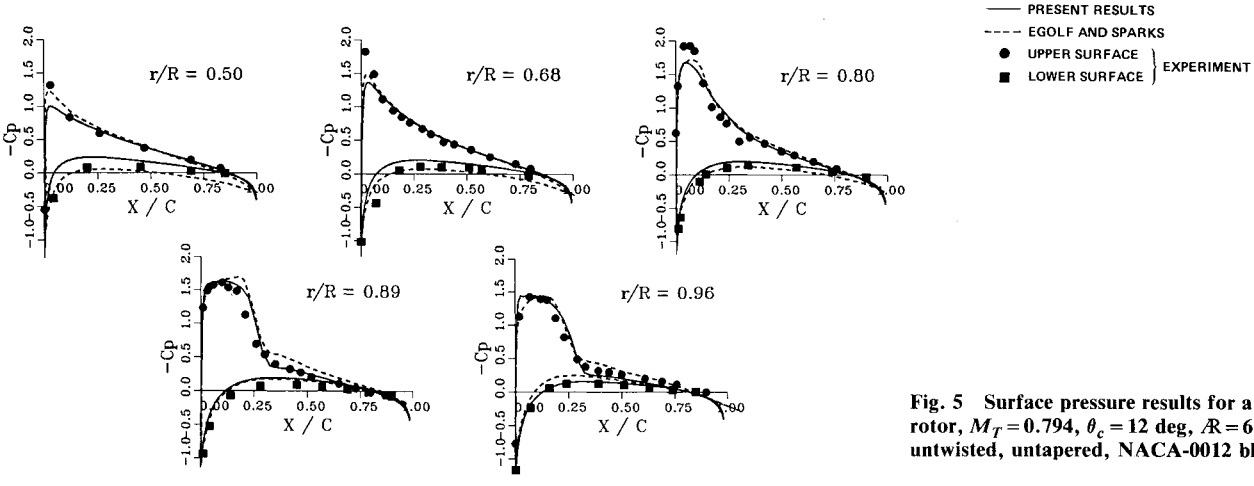

Fig. 5 Surface pressure results for a hovering rotor, $M_T = 0.794$, $\theta_c = 12$ deg, $\mathcal{R} = 6.0$, untwisted, untapered, NACA-0012 blade.

proximately 0.03 chords of rotor motion per time step. Doubling the time step showed no discernible difference in the computed results.

The results from both of these transonic rotor cases indicate the importance of the unsteadiness in the proper prediction of the shock motion. Away from the rotor tip, a quasisteady flow model predicts pressure distributions that are symmetrical at about $\psi = 90$ deg. However, both the data and the computation show no such symmetry. Hence, a quasisteady flow model is not appropriate for a transonic advancing rotor.

Wake Modeling for Hovering Rotors

Proper modeling of wake-induced inflow is a primary problem of rotor flow computations. Prediction of the flow on a hovering lifting rotor is a good initial test of a proposed model. Such a flow has the simplification of being steady. However, the wake from previous blades is close enough to the blade that simple angle-of-attack considerations will not suffice for finite-difference computations.

The load distribution of a hovering rotor is determined by the detailed geometry of the wake. This geometry consists of a complex system of vorticity sheets and tip vortices as shown in Fig. 1. Currently this wake geometry is not reliably predicted except by the use of established data bases appropriate to the particular rotor under consideration. Therefore it will be necessary to empirically specify the most important wake elements (especially the tip vortex locations) as some function of the computed solution.

Our basic approach to this wake modeling is to separate the rotor-wake system into two parts. The first, and most important part, includes the vortices that pass through the finite-difference computational grid. Typically, tip vortices are sufficiently close to the blade so that several will pass through a blade-fixed finite-difference grid. These vortices must be explicitly modeled in the finite-difference solution procedure. The second part of the wake system consists of those vorticity elements that lie outside the finite-difference computational grid. These vortex elements can be modeled with an inflow boundary condition to the full-potential code.

Our approach to modeling the vortex elements in the finite-difference grid is obtained by considering the difference equation [Eq. (8)], which, for convenience, is expressed in functional form as

$$L(\rho^n, \Phi^n, \Phi^{n+1} - \Phi^n) = R(\rho^n, \rho^{n-1}, \Phi^n, \Phi^{n-1}, \Phi^{n-2})$$

$$\rho^n = F(\Phi^n) \tag{12}$$

where the first relation represents mass conservation and the second relation is the Bernoulli equation. Note that the L operator in Eq. (12) is linear with respect to $\Phi^{n+1} - \Phi^n$. This is a result of the original density linearization.

The total potential Φ is now rewritten as the sum of two parts. The first is a known potential, G, which is due to a specified system of vortex elements. The second component is an unknown potential, ϕ, which is the perturbation of G that is due to the rotor and its immediate shed vorticity. If we now substitute the equality $\Phi = G + \phi$ into Eq. (12), the

following form results:

$$L(\rho^n,\Phi^n,\phi^{n+1}-\phi^n)=R\begin{bmatrix}\rho^n,\rho^{n-1}\\ \phi^n+G^n\\ \phi^{n-1}+G^{n-1}\\ \phi^{n-2}+G^{n-2}\end{bmatrix}+L(\rho^n,\Phi^n,G^{n+1}-G^n)$$

$$\rho^n=F(\phi^n+G^n) \tag{13}$$

The left-hand side of Eq. (13) is identical to the original algorithm. The right-hand side and the Bernoulli relation undergo only minor modifications.

For the hover problem, the right-hand functions in Eq. (13) contain only spatial gradient terms in G. Thus, the present scheme amounts to specifying a known velocity field throughout the grid. Strictly speaking, this velocity field must be irrotational since it is derived from the gradient of the potential G. In practice, we include a small rotational core in our vortex velocity fields in order to prevent the velocities from becoming infinite at the vortex centers.

Similar schemes to the one described here have been employed by Steinhoff and Suryanarayanan,[12] Steinhoff et al.,[13] McCroskey and Goorjian,[14] Egolf and Sparks,[8] and Sankar and Malone.[15] The work of Egolf and Sparks is especially pertinent because it treats the same hover problem that is considered here.

The wake elements that lie outside of the finite-difference grid make a large contribution to the total inflow. These elements could be treated by means of a G function obtained from a Biot-Savart computation. This computation would be prohibitively costly because of the large number of grid points and wake elements involved. However, such an approach is unnecessary. The relevant wake elements are far enough from the blade and the resultant velocity gradients are sufficiently small so that the inflow can be handled solely by an inflow boundary condition modification. In the present treatment, this modification takes the form of an angle-of-attack change caused by the outer vorticity field. In the alternate treatment of Ref. 8, the inflow caused by the outer vorticity region is found by an equivalent approach of specifying an induced flow on the outer grid boundary.

Lifting Rotor Computations

We choose to validate our full-potential code and wake-modeling scheme by computing the hovering rotor cases that were experimentally tested in Ref. 16. As mentioned earlier, the computation of hovering flows requires an accurate knowledge of the tip-vortex locations. Although a number of high-speed pressure instrumented rotors have been tested, most of these do not have detailed data on the vortex locations. Thus they are essentially useless for the validation that we require.

The only suitable data for our comparisons are those taken from the Caradonna and Tung hover experiment.[16] This test involved a very stiff two-bladed rotor that was pressure-instrumented in detail at five radial locations. Pressure data were obtained for a range of collective angles and tip Mach numbers up to $M_T=0.877$. Simultaneous measurements of the tip-vortex geometry and strength were made for a sufficient number of cases to establish a wake data base for the entire set of loading conditions. It is these wake data which must be accurately used to compute the rotor loads.

In the present code, the G function in Eq. (13) is found by using two straight infinite vortices located at the experimentally determined locations. The inflow from the remaining vorticity outside the grid is found using a modified version of the A.M.I. code, HOVER,[17] from which the grid contained vorticity elements have been excised. Care is taken to ensure that the thrust and lift values used in the HOVER wake correlations are consistent with those calculated by the finite-difference code. Grid size and outer boundary locations are the same as those used for the previous unsteady calculations.

A comparison of the present computation with a high-speed hover case ($M_T=0.877$, $\theta_c=8$ deg) is shown in Fig. 4. Also included in this figure is a similar full-potential computation from Ref. 8 and a small disturbance calculation from Ref. 18. The three computations show good agreement with the experimental data. The largest discrepancies occur at the inboard blade location. These inboard locations are more affected by the far-field wake model than by the near-field vortices that are located close to the blade tip. All three predictions show a shock location somewhat aft of the measurements. This discrepancy may stem from the lack of a boundary-layer correction.

An interesting aspect of the good comparison between the three codes is that only the present FPR computation and that of Ref. 18 use the measured tip-vortex locations. Egolf and Sparks[8] compute their tip-vortex locations using the Kocurek and Tangler[19] correlations. Our computations have shown that the inboard pressures are significantly altered when the vortex locations are moved solely in the spanwise or normal direction to the rotor. For certain combinations of spanwise and normal motion, however, the inboard pressures are changed very little. This seems to be the case with the Egolf and Sparks results. We found that the experimentally measured tip-vortex locations presented the best comparison to measured pressures. Our experience with the small-disturbance code in Ref. 18 supports this conclusion.

Figure 5 shows a similar comparison of predicted pressures to the Caradonna and Tung[16] hover data for a collective angle of 12 deg. This case represents a more difficult prediction because of the higher lift and stronger vorticity field. A similar prediction from Egolf and Sparks[8] is also shown. The small disturbance code in Ref. 18 could not compute this case because of the high angles of attack involved. As in the previous case, both computer codes compare well with experimental data. Again, we found some sensitivity to the wake modeling. The experimentally consistent wake presented the best comparison to the data.

Conclusions

1) A three-dimensional conservative full-potential equation computer code has been developed for calculating unsteady rotor problems. Good results have been obtained for a nonlifting rotor in forward flight. Lifting cases with vortex interactions will be studied in future work.

2) A "split potential" formulation has been developed which incorporates known vorticity fields into the full-potential calculation. This formulation provides a general method for computing rotor-vortex interaction problems for both steady and unsteady flows.

3) The full-potential code has been coupled with an integral wake model to give good pressure predictions for lifting rotors in hover. An important part of this formulation is an accurate knowledge of the wake geometry, particularly the locations of the first two tip vortices below the rotor. These locations were obtained experimentally in the cases that we considered.

Acknowledgments

The authors would like to thank Dr. Chee Tung of the Army Aeroflightdynamics Directorate for his assistance with the rotor-wake modeling. We would also like to thank Mr. Henry Jones, also of the Army Aeroflightdynamics Directorate, for his useful discussion of much of this work.

References

[1]Caradonna, F. X. and Phillippe, J. J., "The Flow Over a Helicopter Blade Tip in the Transonic Regime," *Vertica*, Vol. 2, April 1978, pp. 43–60.

[2]Phillippe, J. J. and Chattot, J. J., "Experimental and Theoretical Studies on Helicopter Blade Tips at ONERA," *Sixth European Rotorcraft Forum*, Bristol, England, Paper 46, Sept. 1980, pp. 16-19.

[3]Arieli, R. and Tauber, M. E., "Computation of Subsonic and Transonic Flow about Lifting Rotor Blades," AIAA Paper 79-1667, Aug. 1979.

[4]Chang, I-Chung and Tung, C., "Numerical Solution of the Full-Potential Equation for Rotors and Oblique Wings using a New Wake Model," AIAA Paper 85-0268, Jan. 1985.

[5]Bridgeman, J. O., Steger, J. L., and Caradonna, F. X., "A Conservative Finite-Difference Algorithm for the Unsteady Transonic Potential Equation in Generalized Coordinates," AIAA Paper 82-1388, Aug. 1982.

[6]Sankar, N. L. and Prichard, D., "Solution of Transonic Flow Past Rotor Blades Using the Conservative Full-Potential Equation," AIAA Paper 85-5012, Oct. 1985.

[7]Strawn, R. C. and Tung, C., "The Prediction of Transonic Loading on Advancing Helicopter Rotors," *AGARD/FDP Symposium on Applications of Computational Fluid Dynamics in Aeronautics*, Aix-en-Provence, France, Paper 7, April 1986 (also, NASA TM-88238, April 1986).

[8]Egolf, T. A. and Sparks, S. P., "Hovering Rotor Airload Prediction Using a Full-Potential Flow Analysis with Realistic Wake Geometry," *41st Annual Forum of the American Helicopter Society*, Ft. Worth, TX, May 1985, pp. 515-530.

[9]Chang, I-Chung, "Transonic Flow Analysis for Rotors, Part 2 Three-Dimensional, Unsteady, Full-Potential Calculations," NASA TP 2375, Jan. 1985.

[10]Caradonna, F. X., Laub, G. H., and Tung, C., "An Experimental Investigation of the Parallel Blade-Vortex Interaction," *10th European Rotorcraft Forum*, The Hague, the Netherlands, Paper 4, Aug. 1984; also, NASA TM-86005, Nov. 1984.

[11]Tung, C. and Chang, I. C., "Rotor Transonic Computation with Wake Effect," *Fourth International Conference on Applied Numerical Mcdeling*, Taiwan, China, Paper D-23, Dec. 1984.

[12]Steinhoff, J. and Suryanarayanan, K., "The Treatment of Vortex Sheets in Compressible Potential Flow," AIAA Paper 83-1881, 1983.

[13]Steinhoff, J., Ramachandran, K., and Suryanarayanan, K., "The Treatment of Convected Vortices in Compressible Potential Flow," *AGARD Symposium on Aerodynamics of Vortical Type Flows in Three-Dimensions*, AGARD-CPP-342, Rotterdam, the Netherlands, April 1983.

[14]McCroskey, W. J. and Goorjian, P. M., "Interactions of Airfoils with Gusts and Concentrated Vortices in Unsteady Transonic Flow," AIAA Paper 83-1691, July 1983.

[15]Sankar, N. L. and Malone, J. B., "Unsteady Transonic Full Potential Solutions for Airfoils Encountering Vortices and Gusts," AIAA Paper 85-1710, July 1985.

[16]Caradonna, F. X. and Tung, C., "Experimental and Analytical Studies of a Model Helicopter Rotor in Hover," NASA TM-81232 or USAAVRADCOM TR-81-1-23, Sept. 1981.

[17]Summa, J. M. and Clark, D. R., "A Lifting-Surface Method for Hover/Climb Loads," *35th Annual Forum of the American Helicopter Society*, Paper 79-1, Washington, DC, May 1979.

[18]Caradonna, F. X., Desopper, A., and Tung, C., "Finite Difference Modeling of Rotor Flows Including Wake Effects," *Eighth European Rotorcraft Forum*, Aix-en-Provence, France, Paper 2.7, Aug. 1982.

[19]Kocurek, J. D. and Tangler, J. L., "A Prescribed Wake Lifting Surface Hover Performance Analysis," AHS Paper 1001, May 1976.